Supporting Information

Synthesis of Component-Controllable Monolayer $Mo_xW_{(1-x)}S_{2y}Se_{2(1-y)}$ Alloys with Continuously Tunable Band Gap and Carrier Type

You Li[1,2], Kangkang Wang [2], Yiwen Wang[1], Wenbin Huang, Junqi Wang[1], Qichao Yang[1], Ziyue Qian[2], Honggang Wang[2], Junyi Liao[2], Sabir Hussain[2], Liming Xie[2] and Junjie Qi[1*]

[1] *School of Materials Science and Engineering, University of Science and Technology Beijing, Beijing 100083, PR China*

[2]*School of Nanoscience and Technology, University of Chinese Academy of Sciences, Beijing 100049, PR China*

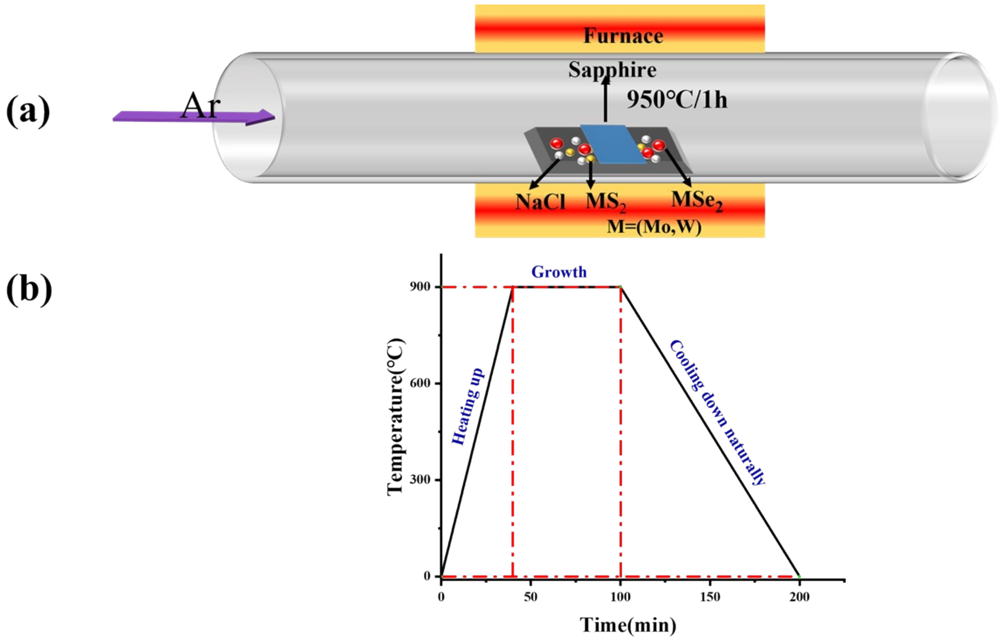

Figure S1. (a) Schematic illustration of the single-heating-zone furnace for the synthesis of monolayer $Mo_xW_{(1-x)}S_{2y}Se_{2(1-y)}$ alloys. (b) Temperature profiles of the samples during growth.

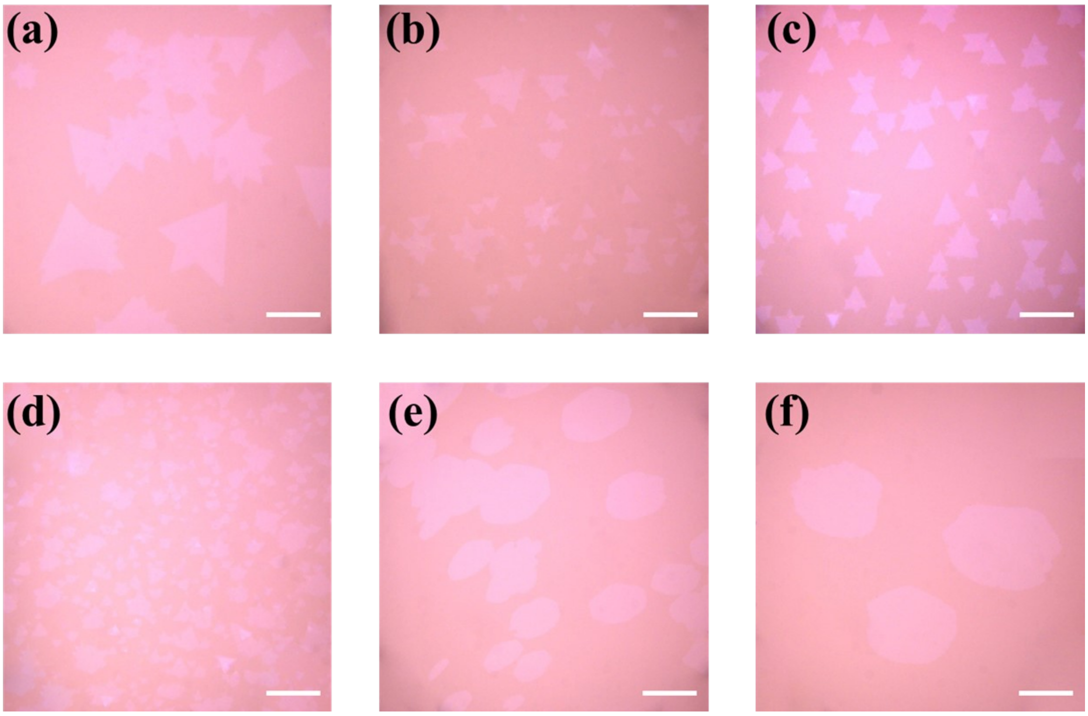

Figure S2. OM images of monolayer $Mo_xW_{(1-x)}S_{2y}Se_{2(1-y)}$ alloys. (a) $Mo_{0.82}W_{0.18}S_{0.28}Se_{1.72}$; (b) $Mo_{0.69}W_{0.31}S_{0.62}Se_{1.38}$; (c) $Mo_{0.50}W_{0.50}S_{0.92}Se_{1.08}$; (d) $Mo_{0.39}W_{0.61}S_{1.20}Se_{0.80}$; (e) $Mo_{0.26}W_{0.74}S_{1.44}Se_{0.56}$; (f) $Mo_{0.10}W_{0.90}S_{1.64}Se_{0.36}$. Scale bar 100 μm.

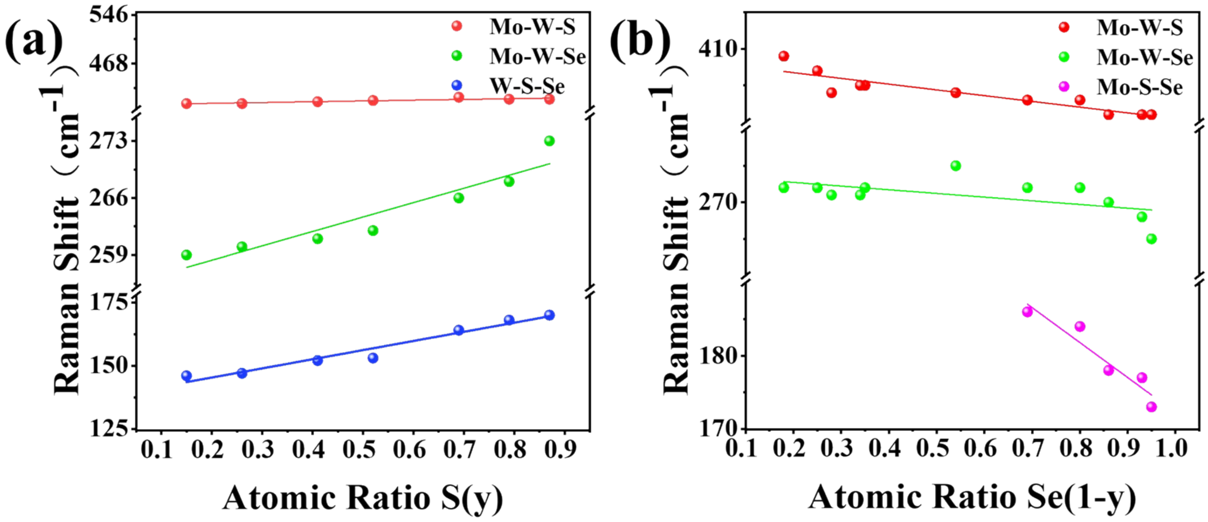

Figure S3. (a) Composition-dependent Raman frequencies of $Mo_xW_{(1-x)}\ S_{2y}Se_{2(1-y)}$ with different weight ratios of MoS_2 and WSe_2 as growth sources. (b) Composition-dependent Raman frequencies of $Mo_xW_{(1-x)}\ S_{2y}Se_{2(1-y)}$ with different weight ratios of $MoSe_2$ and WS_2 as growth sources.

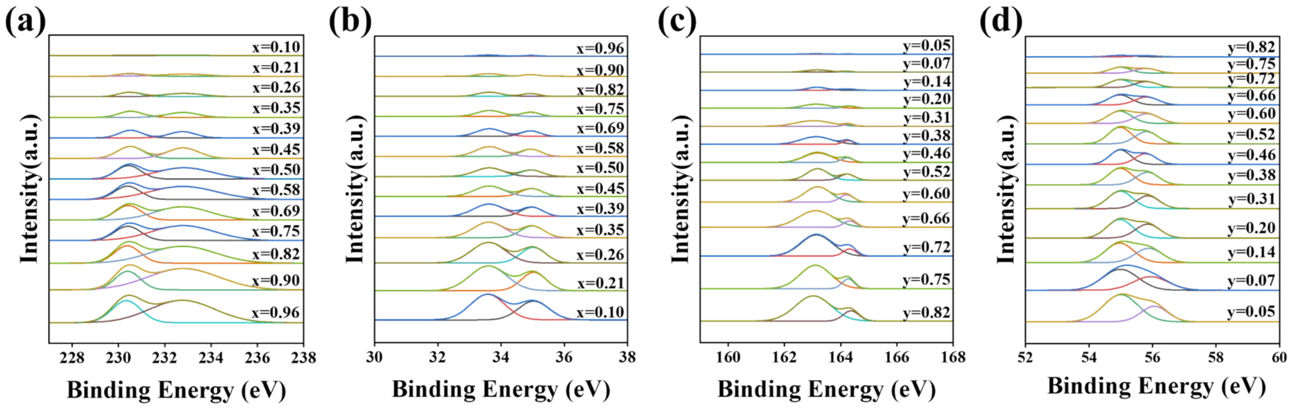

Figure S4. Composition-dependent XPS spectra of monolayer $Mo_xW_{(1-x)}\ S_{2y}Se_{2(1-y)}$ alloys with different weight ratios of MoS_2 and WSe_2 as growth source. (a) Mo 3d, (b) W 4f, (c) S 2p and (d) Se 3d.

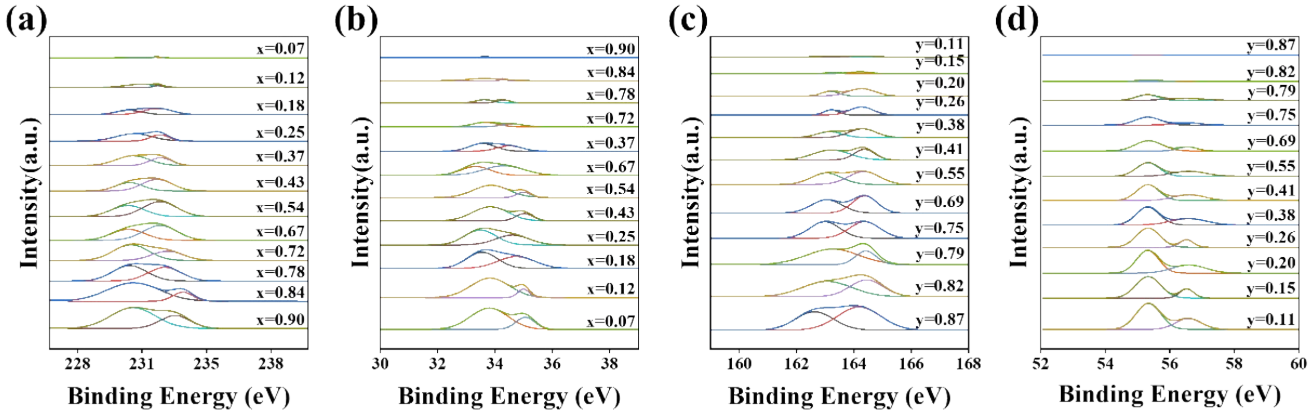

Figure S5. Composition-dependent XPS spectra of monolayer $Mo_xW_{(1-x)}S_{2y}Se_{2(1-y)}$ alloys with different weight ratios of $MoSe_2$ and WS_2 as growth source. (a) Mo 3d, (b) W 4f, (c) S 2p and (d) Se 3d.

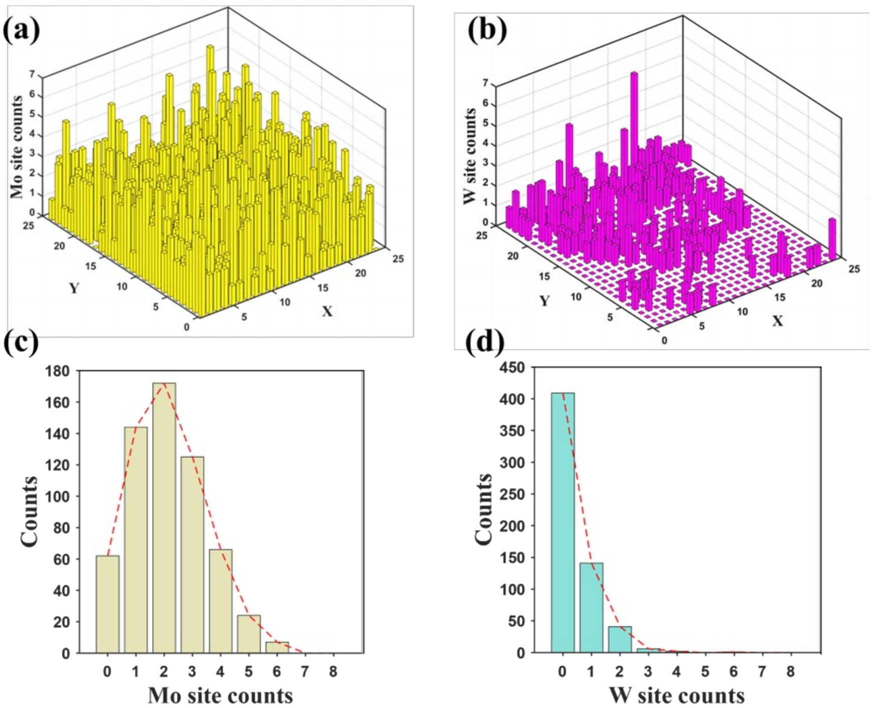

Figure S6. STEM analysis of monolayer $Mo_xW_{(1-x)}S_{2y}Se_{2(1-y)}$ alloy. (a-b) The site distribution histograms of Mo and W in monolayer $Mo_{0.82}W_{0.18}S_{0.28}Se_{1.72}$ alloy, respectively. The image was divided into 25 × 25 parts. (c-d) The corresponding statistical histograms of Mo-site and W-site counts in each part of STEM image.

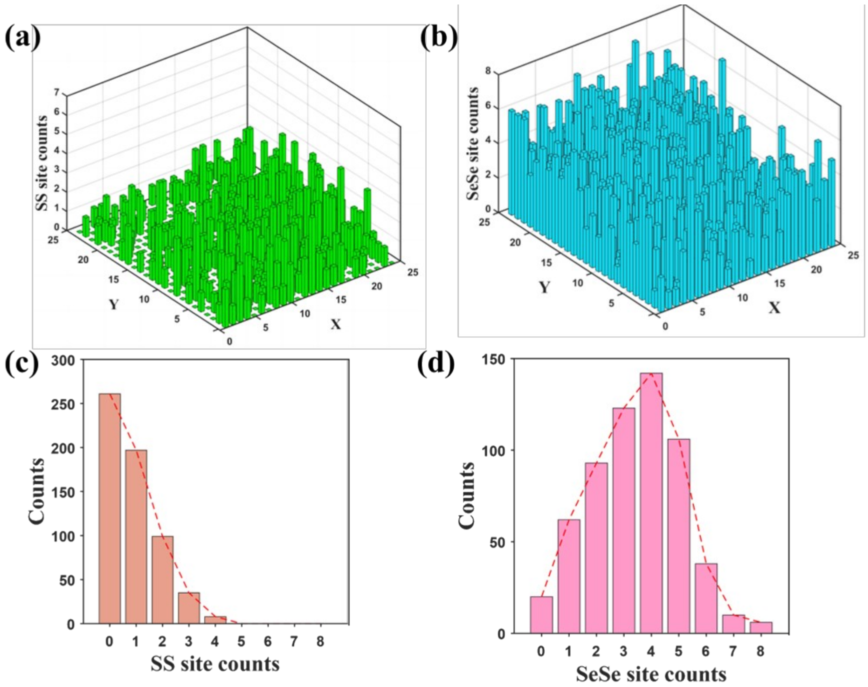

Figure S7. STEM analysis of monolayer $Mo_xW_{(1-x)}S_{2y}Se_{2(1-y)}$ alloy. (a-b) The site distribution histograms of SS and SeSe in monolayer $Mo_{0.82}W_{0.18}S_{0.28}Se_{1.72}$ alloy, respectively. The image was divided into 25 × 25 parts. (c-d) The corresponding statistical histograms of SS-site and SeSe-site counts in each part of STEM image.

Table S1. Summary of monolayer $Mo_xW_{(1-x)}S_{2y}Se_{2(1-y)}$ alloys synthesized with MoS_2 and WSe_2.

Mass Ratio	Atomic Ratio Mo(x)	Atomic Ratio S(y)
m_{MoS_2/WSe_2}=9:1	0.90	0.87
m_{MoS_2/WSe_2}=7.5:1	0.84	0.82
m_{MoS_2/WSe_2}=6:1	0.78	0.79
m_{MoS_2/WSe_2}=4.5:1	0.72	0.75
m_{MoS_2/WSe_2}=3:1	0.67	0.69
m_{MoS_2/WSe_2}=1:1	0.54	0.55
m_{MoS_2/WSe_2}=1:2	0.43	0.41
m_{MoS_2/WSe_2}=1:3	0.37	0.38
m_{MoS_2/WSe_2}=1:4.5	0.25	0.26
m_{MoS_2/WSe_2}=1:6	0.18	0.20
m_{MoS_2/WSe_2}=1:7.5	0.12	0.15
m_{MoS_2/WSe_2}=1:9	0.07	0.11

Table S2. Summary of monolayer $Mo_xW_{(1-x)}S_{2y}Se_{2(1-y)}$ alloys synthesized with $MoSe_2$ and WS_2.

Mass Ratio	**Atomic Ratio Mo(x)**	**Atomic Ratio S(y)**
$\mathbf{m_{MoSe_2/WS_2}=9:1}$	**0.96**	**0.05**
$\mathbf{m_{MoSe_2/WS_2}=7.5:1}$	**0.90**	**0.07**
$\mathbf{m_{MoSe_2/WS_2}=6:1}$	**0.82**	**0.14**
$\mathbf{m_{MoSe_2/WS_2}=4.5:1}$	**0.75**	**0.20**
$\mathbf{m_{MoSe_2/WS_2}=3:1}$	**0.69**	**0.31**
$\mathbf{m_{MoSe_2/WS_2}=2:1}$	**0.58**	**0.38**
$\mathbf{m_{MoSe_2/WS_2}=1:1}$	**0.50**	**0.46**
$\mathbf{m_{MoSe_2/WS_2}=1:2}$	**0.45**	**0.52**
$\mathbf{m_{MoSe_2/WS_2}=1:3}$	**0.39**	**0.60**
$\mathbf{m_{MoSe_2/WS_2}=1:4.5}$	**0.35**	**0.66**
$\mathbf{m_{MoSe_2/WS_2}=1:6}$	**0.26**	**0.72**
$\mathbf{m_{MoSe_2/WS_2}=1:7.5}$	**0.21**	**0.75**
$\mathbf{m_{MoSe_2/WS_2}=1:9}$	**0.10**	**0.82**